Protein−DNA Binding Correlates with Structural Thermostability for the Full-Length Human p53 Protein†

Nicole Magnasco Nichols and Kathleen Shive Matthews*

Department of Biochemistry and Cell Biology, Rice University, Houston, Texas 77005

Received September 5, 2000; Revised Manuscript Received January 25, 2001

ABSTRACT: Full-length p53 protein purified from *Escherichia coli* in the unmodified, "latent" form was examined by several methods to correlate thermal stability of structure with functional DNA binding. Structure prediction algorithms indicate that the majority of β-sheet structure occurs in the p53 core DNA binding domain. Circular dichroism spectra demonstrate that the intact protein is surprisingly stable with a midpoint for the irreversible unfolding transition at ∼73 °C. Significant β-sheet structural signal remains even to 100 °C. The persistent β-sheet CD signal correlates with significant DNA binding (K_d ∼ nM range) to temperatures as high as 50 °C. These data confirm the ability of the DNA binding domain in the full-length "latent" protein to bind consensus dsDNA targets effectively in the absence of activators over a broad temperature range. In addition, we demonstrate that Ab1620 reactivity is not directly correlated with the functional activity of the full-length protein since loss of this epitope occurs at temperatures at which significant specific DNA binding can still be measured.

The p53 protein, originally isolated in mutant form as an oncogene (*1*−*5*), is now known to be crucial for the prevention of tumor formation in humans (reviewed in refs *6*−*9* and references within). The ability of p53 to bind to specific double-stranded DNA (dsDNA) segments and to act as a transcription factor in response to DNA damage is essential for its protective function (*10*−*16*). The majority of p53 mutants isolated from human tumors produce proteins with abrogated dsDNA binding function, reflecting the importance of DNA binding for in vivo functions (*17*−*22*).

Under normal cellular conditions, p53 is maintained at low concentrations through ubiquitin-mediated degradation regulated by interaction with MDM2, an E3 ubiquitin ligase (*23*−*28*). Upon DNA damage, p53 degradation decreases, and cellular levels of p53 increase (*24*, *25*, *27*−*30*). In addition to elevated p53 levels, DNA damage also results in post-translational modifications that alter DNA binding and transcriptional regulation (*6*, *13*, *29*, *30*). In fact, in vitro experiments have demonstrated the requirement for an activating agent (e.g., C-terminal antibody binding, phosphorylation, acetylation) to achieve high affinity dsDNA binding by p53 (*31*−*34*). Consequently, the protein was deduced to exist naturally in a "latent" form with diminished DNA binding ability until activated by a variety of mechanisms. However, in vivo studies have suggested that blocking MDM2-induced degradation of p53 is sufficient to result in an "activated" p53 phenotype (*35*−*39*).

An alternative explanation for the apparent activation requirement has been presented based on the effects of nonspecific competitor DNA present in the most commonly used assay conditions (*40*, *41*). Added nonspecific DNA, including both plasmid DNA (pBluescript) and poly d(I−C), inhibits specific dsDNA binding, apparently by affecting the C-terminus of the p53 protein (*40*, *41*). Because of the presence of these nonspecific competitors, p53 requires artificial "activation" by C-terminal antibody binding, phosphorylation, or other agents to relieve the negative effects of nonspecific DNA. These "activating agents" can therefore be considered "anti-inhibitors", blocking the inhibition of specific DNA binding by nonspecific DNA. Collectively, these data call into question the validity of the commonly accepted "latent-activated" switch hypothesis. Herein, a quantitative determination of the dsDNA binding properties of full-length "latent" unmodified p53 casts further doubt on the necessity for DNA binding activators.

On the basis of both in vivo and in vitro results, full-length, "latent" p53 protein has been deduced to be relatively unstable, in terms of both degradation and folded structure. In response to DNA damage, the half-life of p53 is increased from <30 min to hours (*27*, *29*, *42*). The in vivo half-life of p53 may depend not only on the rate of MDM2-mediated degradation, but also on p53 conformational stability (*43*). Examination of dsDNA binding in the presence of competing nonspecific DNA showed significantly diminished protein activity at 37 °C and higher (*44*, *45*). Loss of reactivity between 37 and 42 °C with Ab1620, an antibody widely used as a determinant for folded and active p53 protein (*46*, *47*), has also been reported (*48*). Further, unfolding studies of the isolated DNA binding domain yielded a T_m of ∼42 °C (*49*). These observations have provided support for the hypothesis that intact p53 is not a thermodynamically stable

† This work was supported by grants from the G. Harold and Leila Y. Mathers Foundation and the Robert A. Welch Foundation (C-576). N.M.N. was supported by an NIH Molecular Biophysics Training Grant (GM-08280). Spectroscopic facilities were provided by the Keck Center for Computational Biology and the Lucille P. Markey Charitable Trust.

* To whom correspondence should be addressed. Phone: 713-348-4871; fax: 713-348-6149; e-mail: ksm@bioc.rice.edu.

10.1021/bi002088z CCC: $20.00
Published on Web 03/06/2001

protein and that its DNA binding activity therefore exhibits thermal sensitivity (*44*, *45*, *48*, *50*, *51*).

We have used circular dichroism (CD) in conjunction with sequence-based structure prediction algorithms to examine the secondary structure of full-length p53 produced in *Escherichia coli* without the posttranslational modifications that occur in eukaryotic organisms. In contrast to expectations from previous domain studies, the intact, full-length protein is surprisingly thermostable, with an estimated transition midpoint of ~73 °C. CD signal corresponding to significant amounts of β-sheet structure persists to temperatures as high as 100 °C. Further, at temperatures up to 50 °C, the bacterially derived, "latent" p53 demonstrates high affinity dsDNA binding to its consensus sequence that requires no "activation". However, we did observe loss of Ab1620 antibody reactivity between 37 and 42 °C, similar to behavior observed previously (*48*). These data suggest that the stable β-sheet structure observed by CD reflects a folded and active DNA binding domain that persists even after loss of reactivity with Ab1620. We conclude that, in the context of the full-length, unmodified protein, the DNA binding domain maintains a much more stable structure than previously presumed and that Ab1620 reactivity does not correlate directly with specific dsDNA binding capacity.

MATERIALS AND METHODS

Plasmids and Cell Strains. The human p53 gene cloned into the pET15b expression plasmid and hybridoma cells expressing the monoclonal p53 antibody Ab421 were generous gifts from the laboratory of Dr. G. Lozano (M. D. Anderson Cancer Center, Houston, TX). The p53 gene was excised from pET15b and cloned into a pRSET plasmid using *Xba*I and *Bam*HI restriction enzyme sites. Bacterial strain DH5α was used to prepare all double stranded DNAs. BL21(DE3) cells, with or without the pLysS episome (Novagen), were used for p53 expression.

Protein Purification and Determination of Assembly. Cells transformed with pRSET plasmid containing wild-type human p53 were grown overnight on LB agar plates supplemented with 50 μg/mL ampicillin. Individual colonies were transferred into 12 L of LB media containing ampicillin, and the bacteria were allowed to grow slowly overnight with moderate shaking (~32 °C at ~150 rpm) to maximize soluble protein production. When the cells had reached an absorbance at 600 nm of 0.6−0.8, IPTG was added to 1 mM to induce protein production, and the cultures were allowed to shake gently at room temperature (~100 rpm). Cells were harvested 4 h post-induction and resuspended in 20−30 mL of breaking buffer containing 0.01 M $Mg(CH_3COO)_2$, 1 mM $Zn(CH_3COO)_2$, 0.1 M Tris-HCl, pH 7.6, 0.3 M KCl, 5 mM DTT,[1] 1 mM PMSF, and 10% (v/v) glycerol and frozen overnight in the presence of ~0.4 mg/mL lysozyme at −20 °C.

After thawing and complete cell lysis, a trace amount of DNaseI was added and the mixture was allowed to incubate for 30 min. The cell debris was removed by centrifugation. Ammonium sulfate was added slowly to 20% saturation, and the suspension was allowed to sit for 1 h at 4 °C. The solution was centrifuged, and the pellet was discarded. Ammonium sulfate was added to the supernatant to 35% saturation, and this mixture was allowed to precipitate overnight at 4 °C. Following centrifugation, the pellet was resuspended in <5 mL of 0.2 M KPB [potassium phosphate buffer, pH 7.5, 5 mM DTT, 10% (v/v) glycerol and 5% (w/v) glucose] and dialyzed against 0.2 M KPB for 2 h with three buffer changes. Overnight dialysis was avoided since it resulted in significant protein loss. The dialysate was then loaded onto a small, ~2 mL phosphocellulose column, and p53 protein was eluted midway through a 0.2−0.5 M KPB gradient. Fractions were confirmed to contain p53 by Western analysis with either monoclonal antibody Ab421 (*52*) or Ab240 (*53*). Protein purity was determined by SDS−PAGE analysis, and densitometry of the stained protein bands and ranged from ~80−90% per preparation (see Figure 9, lane 2). Protein concentration was determined by a Bio-Rad assay (*54*). Because of dramatic protein loss upon concentration or dialysis, the purified protein samples were used directly in all assays as eluted from the column in ~0.35 M KPB.

Glutaraldehyde cross-linking experiments were conducted at both room temperature and 50 °C to verify that p53 remains tetrameric over this temperature range. Protein at 5.0×10^{-7} M tetramer (MW_{tet} is 188 000) in 0.3 M KPB was incubated with 0.01% glutaraldehyde for 5 or 20 min before samples were prepared and loaded on a step SDS−PAGE of 5 and 7.5%. Gels were either silver stained or transferred onto nitrocellulose to perform Western blotting with Ab240 to confirm p53-containing bands.

Secondary Structure Prediction. Structure prediction algorithms were accessed through the Biology Workbench, Protein Tools (University of Illinois; http://biology.ncsa.uiuc.edu/). Output files were examined for the exact number of amino acids calculated to be involved in either α-helical or β-sheet structure. The determined regions of secondary structure from published NMR and X-ray crystallographic structures were used to calculate the percentage of α-helical and β-sheet structure for the entire protein. The percent contribution to the entire protein was calculated by summing the amino acids for each type of structure. These values were determined using the beginning and ending points of helices and sheets reported in the published structures and dividing by 393, the number of amino acids in a human p53 monomer.

Circular Dichroism. Circular dichroism spectra were collected on an AVIV model 62A DS circular dichroism spectrometer equipped with Star 3.0 Stationary. For these experiments, wild-type p53 was at a protein concentration of 8.0×10^{-7} M tetramer in the buffer in which the protein was purified, ~0.35 M KPB. 10-Camphorsulfonic acid was used as an internal standard. A quartz cuvette with a 0.2-cm path length was used to minimize loss of light due to scatter and absorption of DTT present in the protein sample. Scans were collected in 0.5-nm increments from 255 to 200 nm with an 8 s/point averaging time. Baseline buffer spectra were subtracted from sample spectra prior to averaging the points along each temperature curve. Data points were converted to $\Delta\epsilon$ using Beers Law,

$$\Delta\epsilon = \epsilon(\mathrm{L}) - \epsilon(\mathrm{R}) = \frac{\Delta \mathrm{A}}{cl} \qquad (1)$$

[1] Abbreviations: BSA, bovine serum albumin; DTT, dithiothreitol; IPTG, isopropyl-β-D-galactopyranoside; LB, Luria broth; PMSF, phenylmethanesulfonyl fluoride; Pu, purine; Py, pyrimidine.

where c is the concentration of p53 expressed in M tetramer, l is the cuvette path length in cm, and ΔA is the measured CD signal. The spectra were then smoothed ($n = 7$) and plotted in Igor Pro (Wavemetrics).

Temperature was monitored at the sample compartment with a computer-controlled Peltier device. For each temperature, the sample was equilibrated in the cell holder for 3 min before full wavelength (255−200 nm) scans were collected to assess the contributions of both α-helix and β-sheet to the signal. CD spectra of p53 were also collected as a function of time (up to 120 min) to verify that equilibrium was reached at each point in the temperature range investigated (data not shown). Spectra were collected at temperatures ranging from 0 to 100 °C in 10° steps. The results from multiple independent runs were averaged. Similar data were obtained on at least three different protein preparations. Data points at 218 and 210 nm were expressed as a fraction of the initial signal (at 0 °C) as a monitor of β-sheet and α-helical content, respectively. The data were fit to a modified Michaelis−Menten equation to estimate the midpoint of irreversible unfolding. Similar behavior was also observed for protein spectra collected in buffer D [∼0.2 M potassium phosphate buffer, pH 7.5, 2.5 mM DTT, 5% (v/v) glycerol, and 2.5% (w/v) glucose]. Spectra of unfolded p53 were generated by incubation of the protein in ∼7 M guanidine hydrochloride, and data were collected in 1-nm steps with a 3 s averaging time. Unfolded p53 spectra were corrected as described above, averaged, and plotted from 210 to 255 nm in Igor Pro. Data collected at wavelengths lower than 210 were complicated by interference from both DTT and guanidine hydrochloride.

Antibody Experiments. Purified p53 protein was diluted into 0.05 M potassium phosphate buffer, pH 7.5, with 0.1 mg/mL BSA yielding a 4.0×10^{-7} M tetramer solution in buffer D with 0.1 mg/mL BSA. Samples were incubated at either 0, 5, 16, 22, 37, 42, 50, or 65 °C for 30 min before rapid filtration at room temperature onto a nitrocellulose filter presoaked in 0.05 M potassium phosphate buffer, pH 7.5. Temperature measurements for samples containing buffer in the absence of protein were used to establish that no significant temperature change occurred during filtration. The nitrocellulose filter was blocked with 10% dry milk in PBST [phosphate buffered saline, pH 7.4, 0.05% (v/v) Tween 20] for 30 min and exposed to either Ab1620 or Ab421 overnight at 4 °C. After thorough washing with PBST, the filter was incubated with a secondary antibody complexed to horseradish peroxidase for 1 h at room temperature followed by PBST washes. The use of an ECL kit (Amersham) and subsequent film exposure allowed visualization of the reaction. Reactivity was quantitated by a Molecular Dynamics Computing Densitometer equipped with ImageQuant software. The reactivity at each temperature was normalized to the reactivity of the 0 °C sample for each experiment.

DNA Binding. A variation of the 96-well nitrocellulose filter assay first described by Wong and Lohman (*55*) was used to determine equilibrium dissociation constants for p53 binding to its consensus sequence, conDNA, as well as to a nonspecific sequence, NS2, under non-stoichiometric conditions. The conDNA sequence, 5′-AGACATGCCTAGACATGCCT, and its complement were commercially synthesized (Great American Gene Co.) and are based on the p53 consensus DNA operator, consisting of two repeats of the 10 base pair motif 5′-PuPuPuC(A/T)(T/A)GPyPyPy (*11*, *12*). DNA binding assays to determine nonspecific DNA binding by p53 employed the 20-mer sequence 5′-TCCAGATGTACCCAAACGTG and its complement. Complementary DNAs were annealed to form double-stranded 20-base pair targets and labeled at the 5′-ends using γ[^{32}P]-ATP and polynucleotide kinase incubated at 37 °C for 1 h. Protein from 1.0×10^{-7} to 1.0×10^{-11} M (tetramer concentration) was incubated with either 2×10^{-11} M conDNA or 2×10^{-10} NS2 DNA, both well below the K_d value of the respective interactions. Buffer used to dilute the protein samples contained 0.1 mg/mL BSA to minimize aggregation and adherence of protein. The protein−DNA samples were incubated for 30 min at the temperature indicated (from 0 to 50 °C) in 0.05 M potassium phosphate buffer (KP), pH 7.5, before rapid filtration through nitrocellulose paper (Schleicher and Schuell). The nitrocellulose was dried at 65 °C for 5 min and then exposed to a phosphorimaging plate at room temperature. A Fuji Phosphorimager was used to quantitate the pixels, and a value for a background point with no protein was subtracted from each corresponding condition with protein (Fuji MacBas Software). Values from multiple sets of experiments were fit (Igor Pro, Wavemetrics) according to the following equation,

$$R = Y_{max} \frac{[p53]^n}{[p53]^n + K_d^n} \quad (2)$$

where R is the amount of bound complex at a specific protein concentration divided by the amount of bound complex at saturating protein, Y_{max} is a correction factor that allows for the R value at saturation to float, K_d is the apparent equilibrium dissociation constant, [p53] is the concentration of p53 protein expressed in tetramer, and n is the Hill coefficient. The value of n (∼1.6) did not vary significantly under any conditions employed in these experiments. Binding data are the compilation of multiple assays over at least two different protein preparations per temperature. DNA binding at temperatures exceeding 50 °C was not possible due to the melting temperature of the dsDNA targets ($T_m \sim 55$ °C).

Protein activity assays were conducted both at room temperature and at 50 °C as described above but with conDNA concentration above the K_d at 2×10^{-8} M and protein concentrations from 3.0×10^{-7} to 1.0×10^{-8} M tetramer. Protein concentrations for each experiment to determine equilibrium dissociation constants were corrected to reflect the relative activity of the sample, which was ∼30−50% for each preparation at both temperatures examined.

Effects of nonspecific DNA sequences and Ab421 on consensus DNA binding were also examined using nitrocellulose filtration. Where indicated, Ab421 was added at 2.4×10^{-8} M (420 ng) just over a stoichiometric concentration to p53, which was held constant at 1×10^{-8} M. Radiolabeled conDNA was then added at 2×10^{-11} M. When present, nonspecific DNA was added last at 2×10^{-6} M, a concentration above the K_d determined for nonspecific binding. The experiments were conducted as indicated for DNA binding analyses with an additional 10 min incubation on ice to allow for Ab421-protein binding prior to the addition of either DNA. Data were corrected to fractional activity of p53−conDNA binding alone at each temperature.

Thermodynamic Analysis of DNA Binding. DNA binding data collected as a function of temperature were analyzed using a van't Hoff plot fit to the following equation modified from Ha et al. (*56*):

$$\log K_{obs} = \frac{\Delta C_{p,obs}}{2.303R}\left(\frac{T_H}{T} - \ln\frac{T_S}{T} - 1\right) \quad (3)$$

where ΔC_p is the change in the heat capacity for the p53−DNA complex formation, K_{obs} is the apparent equilibrium association constant for DNA binding, and T_H and T_S are the temperatures at which ΔH (enthalpy) and ΔS (entropy) are zero, respectively. The subscript "obs" indicates that the thermodynamic values are a function of solution variables, including salt and pH. Thermodynamic parameters for enthalpy, entropy, and Gibbs free energy (ΔG) were calculated from ΔC_p, T_H, and T_S, according to eqs 4−6 (*56*).

$$\Delta H_{obs} = \Delta C_{p,obs}(T - T_H) \quad (4)$$

$$\Delta S_{obs} = \Delta C_{p,obs} \ln \frac{T}{T_S} \quad (5)$$

$$\Delta G_{obs} = \Delta H_{obs} - T\Delta S_{obs} \quad (6)$$

Values for ΔG calculated from eq 6 were compared with values calculated from the experimental data as determined by eq 7.

$$\Delta G_{obs} = -RT\ln K_{obs} \quad (7)$$

RESULTS

Structure Prediction for p53 Correlates Well with Solved Structures. Sequence-based structure prediction algorithms from the Biology Workbench were used to predict the secondary structure elements of the human p53 protein. These predictions were then compared to the previously determined NMR and X-ray crystallographic structures for p53 fragments. A small N-terminal α-helix (residues 17−27, Figure 1, panel A; box 1, Figure 2) of p53 was crystallized with the N-terminus of MDM-2, defining the basis for this interaction (*57*). The DNA binding core domain (DBD, residues 94−312, Figure 1, panel B; box 2, Figure 2) was crystallized as a monomer bound to DNA (*58*). The structure reveals that the DBD is primarily composed of β-sheet structure with small α-helical segments. Both NMR and X-ray crystallography were used to determine that the structure of the C-terminal oligomerization domain (residues 319−356, Figure 1, panel C; box 3, Figure 2) is organized as a dimer of dimers (*59*−*61*). Each dimeric unit contains an antiparallel, two-stranded β-sheet and two antiparallel α-helices with interactions between the dimers strictly limited to the helices. A fourth structure published recently demonstrates that a fragment of p53 C-terminal to the tetramerization domain that is unstructured as a free peptide (residues 376−387, Figure 1, panel D; box 4, Figure 2) forms an α-helix upon binding to the S100B($\beta\beta$) protein dimer (*62*).

The percentage of β-sheet structure identified in p53 from the four structures shown in Figure 1 is ∼19%. Results from two sequence-based structure prediction algorithms, Chou−Fasman (CF) and Garnier−Osguthorpe−Robson (GOR), are shown in Figure 2 (*63*, *64*). Both algorithms predict all four regions of known structure reasonably well. The predicted percentages of β-sheet structure are 19.8 and 17.8% by CF and GOR methods, respectively, indicating that the β-sheet rich DBD and the C-terminal β-sheet in the oligomerization domain account for nearly all β-sheet structure in the full-length protein.

The percentage of α-helix within the known structures is ∼13%, whereas the predicted values for the full-length protein are 18.0% from the GOR and 16.5% from the CF algorithms, suggesting that additional, as yet unsolved, portions of p53 may contain α-helical regions. Five other predictive algorithms from the Biology Workbench yielded similar results and also predicted structure consistent with the solved domains with average predicted values of 18% α-helical and 16% β-sheet structure for full-length p53 (*65*−*69*).

Circular Dichroism Shows p53 Thermostability. The secondary structure of p53 was examined using circular dichroism spectroscopy to determine the effects of increasing temperature on p53 stability. The shape and intensity of the CD spectra of intact purified p53 protein at temperatures less than 60 °C were consistent with a folded protein. Major contributions of both β-sheet and α-helical structure were indicated by the spectral minima observed at ∼218 and 208 nm, respectively (Figure 3). This finding correlates well with the emerging picture of p53 from both structures of individual domains and the prediction algorithms used in this study. The mixed α/β structure can be observed at temperatures from 0 to 60 °C. With increasing temperature, the signal at ∼210 nm that reflects α-helical content gradually decreases until ∼70 °C, at which point the shape of the spectrum is consistent with an all β-sheet protein and minimal α-helical content. Strikingly, significant loss of the β-sheet structure signal at 218 nm is not observed until temperatures exceed 60 °C. The presence of ∼10% glycerol in the sample allowed measurements to be taken at 100 °C where considerable β-sheet structure persists. Attempts to reach temperatures high enough to generate spectra characteristic of random coil were not possible due to substantial sample evaporation. It was therefore necessary to incubate p53 in the presence of ∼7 M guanidine hydrochloride to generate a spectrum for the unfolded protein for comparative purposes (Figure 3).

Thermal unfolding was irreversible (data not shown), consistent with findings reported previously for the core domain alone (*49*). For this reason, thermodynamic calculations of unfolding energies were not possible. However, analysis of the data for β-sheet structure at 218 nm indicates a midpoint of ∼73 °C for the transition (Figure 4), a value that is reproducible over multiple experiments, several preparations of protein, and two different buffer conditions (see Materials and Methods). In an attempt to determine the T_m for the α-helical unfolding transition, data points at 210 nm were examined as a function of temperature (Figure 4). The increased interference of DTT at wavelengths lower than 210 nm precluded examination at 208 nm, a standard wavelength monitored for α-helical structure. The midpoint of the 210 nm data is at ∼68 °C, but this value appears to be a high estimate, as spectra above 60 °C appear to have minimal α-helical content and the baseline is complicated by the presence of the persistent β-sheet signal (see Figure 3). On the basis of both known and predicted structures (Figures 1 and 2), the β-sheet structure signal monitored by

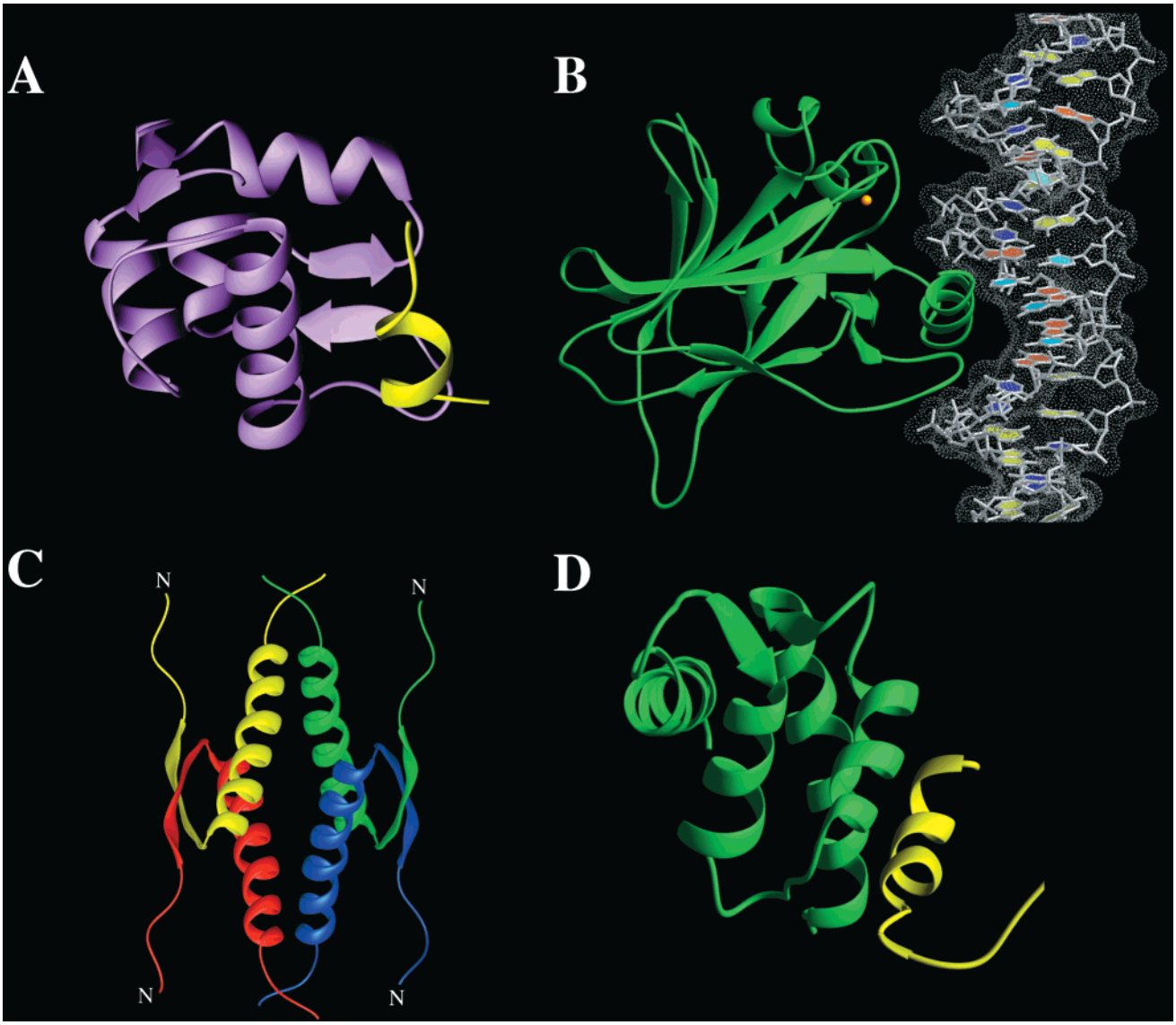

FIGURE 1: X-ray crystallographic and NMR structures for domains of p53. These four structures displayed using Ribbons (*83*) represent ~70% of the p53 protein. (A) An MDM-2 peptide binds to a small N-terminal fragment of p53 (yellow) that forms a small α-helix (residues 17−27) in the complex (*57*). (B) The DNA binding domain (residues 94−312), which has substantial *β*-sheet structure, is shown bound to its dsDNA consensus half-site (*58*). This region contains a crucial zinc atom (orange). (C) The C-terminal oligomerization domain (residues 319−356) forms an antiparallel four-helical bundle anchored by *β*-sheet segments. The N-terminus of each monomer is marked for clarity (*59*−*61*). (D) NMR structure of a domain of the S100B protein bound to residues 376−387 of p53 (yellow). This C-terminal region of p53 is largely unstructured in the absence of S100B but folds into an α-helix upon binding to the S100B protein (*62*). Two domains of p53 interact with the S100B(*ββ*) dimer, but a single monomeric interaction is shown for clarity.

CD can be correlated with the core DNA binding domain of the protein. We therefore conclude that the DNA binding domain in the full-length protein is much more stable than the isolated domain, which has an apparent T_m of 42 °C (*49*).

Latent p53 Can Bind Consensus DNA up to 50 °C. While CD can monitor substantial structural changes in a protein, subtle conformational changes that may influence protein function are not necessarily detectable. We therefore examined the DNA binding activity of p53 as a function of temperature to establish that the significant *β*-structure observed in CD spectra at elevated temperatures corresponded to a functionally intact DNA binding domain. Using a p53 consensus sequence, conDNA, DNA binding was examined at temperatures at which significant *β*-sheet stability was indicated by CD experiments. Consistent with an intact and active core domain, high affinity dsDNA binding by p53 was observed at all temperatures assayed (Table 1, Figure 5, panel A). Measurement of DNA binding at temperatures greater than 50 °C was precluded by the T_m of the 20-bp target sequences. At room temperature, specific p53 DNA binding shows an apparent K_d of 1.6×10^{-9} M tetramer, confirming an intact DNA binding domain. At 42 °C, a temperature at which p53 has been reported to be inactive in the presence of nonspecific DNA competitors (*48*), high affinity binding in the absence of these competitors is still observed. Specific dsDNA binding was observed even at 50 °C, with an apparent K_d of 7.2×10^{-9}, only 6-fold lower than that measured at room temperature (Table 1). Additionally, measurements of activity under stoichiometric conditions indicated no difference in the fraction of active protein at elevated temperatures (data not shown). Thus, the *β*-sheet DNA binding core not only retains significant secondary structure at elevated temperatures, as indicated

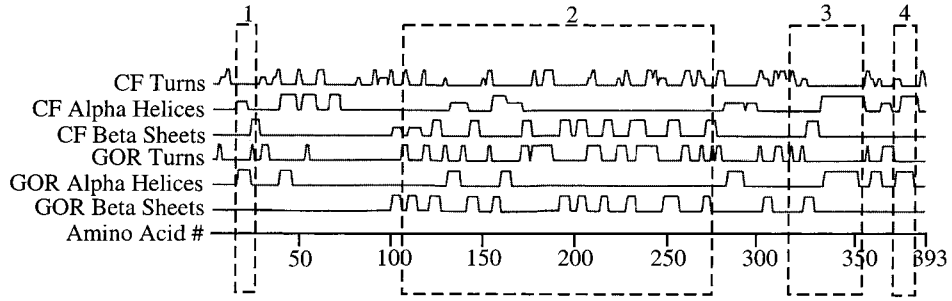

FIGURE 2: Comparison of Chou−Fasman (CF) and Garnier−Osguthorpe−Robson (GOR) structure prediction algorithms to solved structures of p53. The 393-amino acid p53 protein is depicted in linear sequence format. Peaks in each line represent predicted structure of turns, α-helices, or β-sheets, by either CF or GOR algorithms (*63*, *64*). Dashed boxes 1−4 outline the p53 fragments for which a structure has been published: (1) the MDM-2 recognition helix; (2) the β-sheet rich DNA binding domain; (3) the tetramerization domain; and (4) the C-terminal S100B recognition peptide. These four solved structures identify ∼19% β-sheet and ∼13% α-helical structure in p53, whereas the CF and GOR algorithms predict 19.8 and 17.8% β-sheet and 16.5 and 18.0% α-helix, respectively.

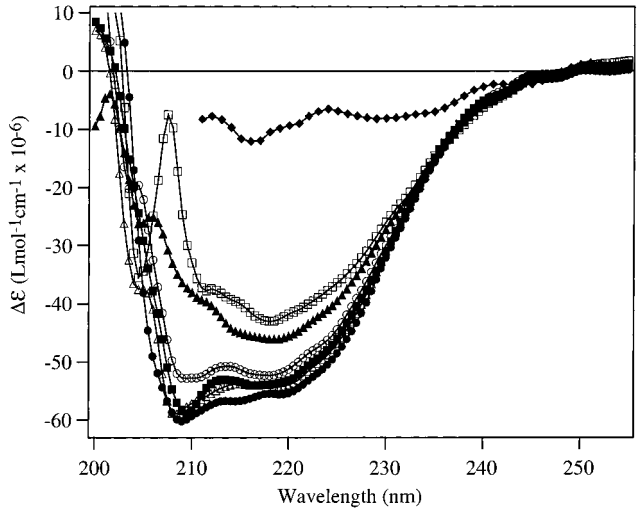

FIGURE 3: Circular dichroism spectra of p53 as a function of temperature. CD spectra were collected on an AVIV model 62A DS instrument from 0 to 100 °C in 10° intervals as described in Materials and Methods. Samples contained purified full-length p53 protein at a concentration of 8.0×10^{-7} M tetramer in 0.35 M KPB. The absorbance of 5 mM DTT present in the protein buffer decreases the signal-to-noise ratio at wavelengths less than 210 nm. Spectra were baseline corrected and smoothed before being plotted. Data points are expressed as a change in extinction coefficient, $\Delta\epsilon$, as determined from eq 1. Samples varying either by protein preparation, buffer condition, or collection times (up to 120 min) all yielded similar results. Spectra are shown in 20 °C intervals. (●) 0 °C, (△) 20 °C, (■) 40 °C, (O) 60 °C, (▲) 80 °C, (□) 100 °C. An average spectrum of p53 unfolded by ∼7 M guanidine hydrochloride is shown for comparison (♦). For this spectrum, wavelengths less than 210 nm are excluded due to the small signal-to-noise ratio.

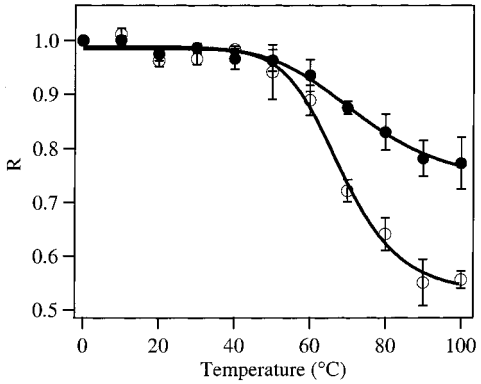

FIGURE 4: Assessment of temperature dependence of α-helical and β-sheet structures in p53. CD data at 218 nm (●) and 210 nm (O) as a function of temperature were averaged ($n = 3$) to assess the fraction of residual structure (R) at wavelengths that monitor β-sheet (218 nm) and α-helical (210 nm) structure. Values are expressed as a fraction of the initial signal at 0 °C. The solid lines are a fit of the data points to a modified Michaelis−Menten equation to determine the midpoint of the unfolding curve. Because thermal unfolding of p53 is irreversible, the resulting transition midpoints of 73 °C at 218 nm and 68 °C at 210 nm are useful primarily for comparative purposes. Error bars indicate one standard deviation.

Table 1: Apparent Equilibrium Dissociation Constants (K_d) for Specific dsDNA Binding as a Function of Temperature

temp (°C)	K_d (M tetramer)[a]
0	$1.7 \pm 0.2 \times 10^{-9}$
10	$1.3 \pm 0.1 \times 10^{-9}$
22	$1.6 \pm 0.1 \times 10^{-9}$
37	$1.9 \pm 0.1 \times 10^{-9}$
42	$3.6 \pm 0.2 \times 10^{-9}$
50	$7.2 \pm 1.1 \times 10^{-9}$

[a] K_d values were determined from the fit of the binding data in Figure 5, panel A, to eq 2. Values reported are the average of at least three independent experiments from at least two different protein preparations.

by the CD data, but this region also remains functionally active.

For comparison to conDNA, a nonspecific DNA (NS2) was designed. This sequence is composed of many of the least used bases at each position of the consensus sequence (*11*), while at the same time maintaining the number of G/C and A/T base pairs. The affinity of p53 to NS2 was sufficiently low that it was not possible to generate complete binding curves (Figure 5, panel B). However, an estimate of the K_d indicated a value $>5 \times 10^{-8}$ M at both room temperature and 50 °C, significantly lower than that for p53−conDNA binding at any measured temperature.

Effect of Nonspecific DNA and C-terminal Antibody on Consensus DNA Binding. Previous studies have demonstrated that nonspecific DNA inhibits p53 binding to consensus DNA sequences and that this effect is mitigated by inclusion of antibody specific for the C-terminal region of p53 in the assay mixture (*40*, *41*). To confirm that the bacterially produced protein examined in this study demonstrated similar behavior, binding studies were performed at 0, 22, and 50 °C. As evident in Figure 6, the addition of 2×10^{-6} M nonspecific DNA, for which binding was measured directly (see Figure 5, panel B), inhibited binding to consensus DNA substantially. Stoichiometric addition of Ab421 restored

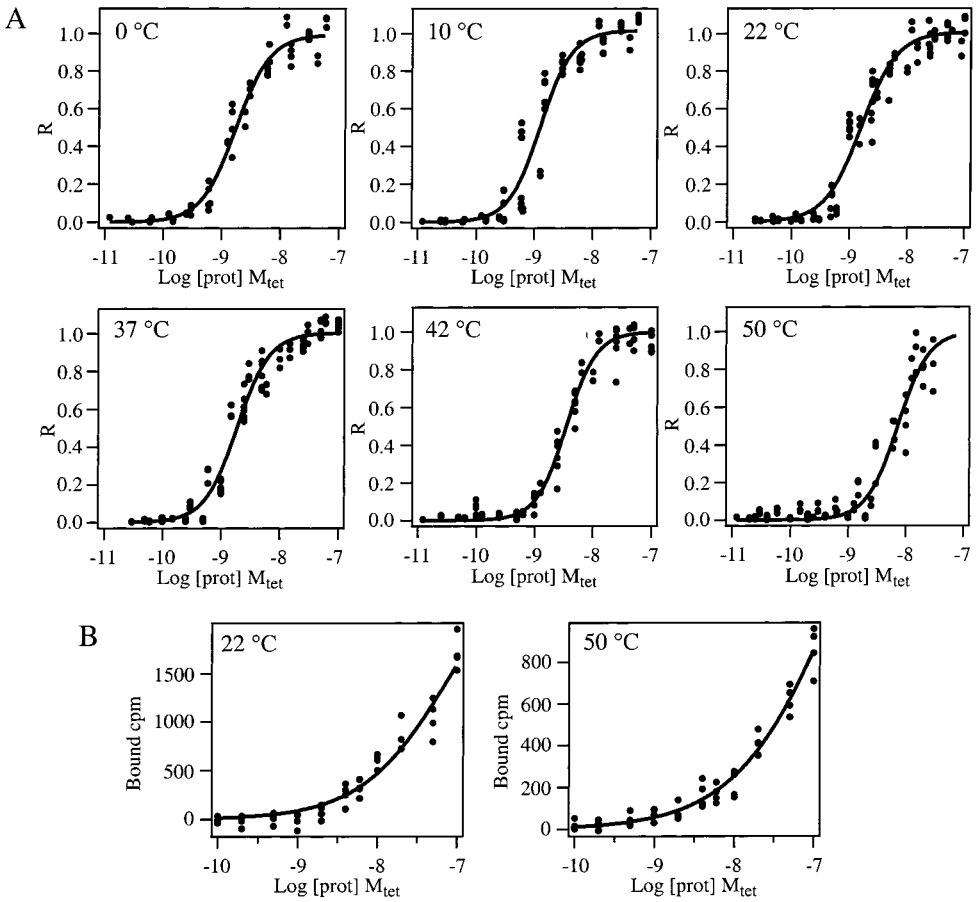

FIGURE 5: p53 DNA binding as a function of temperature. (A) Isotherms for full-length p53 binding to the specific dsDNA target, conDNA, are shown. Protein at the indicated concentration (in M tetramer) was incubated for 30 min at the temperature indicated. Labeled DNA concentration was held constant at 2×10^{-11} M. Data at each temperature were derived from at least three experiments and two protein preparations. The protein concentration was corrected based on measured percent protein activity. Fractional saturation (R) was determined by the amount of bound complex at a specific protein concentration divided by the amount of bound complex at saturating protein. Solid lines are fits to all data points at each temperature to determine the dissociation constant (K_d) for dsDNA binding shown in Table 1. (B) Isotherms for p53-nonspecific DNA (NS2) binding are shown. Experiments were conducted similarly to those for conDNA binding, but fractional saturation data could not be generated in the absence of a measurable saturation level, and bound radioactivity is reported. The estimated K_d values are $>5 \times 10^{-8}$ M and do not appear to vary significantly with temperature.

binding to levels approaching those in the absence of nonspecific DNA, whereas the addition of Ab421 alone had no significant effect on p53−conDNA binding. The behavior observed was similar at all temperatures examined.

Thermodynamic Analysis of DNA Binding Suggests Minimal Conformational Change. For protein−ligand interactions, the heat capacity change of the reaction can be a useful determinant of the amount of conformational rearrangement linked to the binding process (*56*). ΔC_p can be derived from fitting a plot of ln K_a vs $1/T$ (Figure 7). The more concave this curve, the greater the negative change in the heat capacity and the larger the presumed surface area buried in the p53−DNA interaction. ΔC_p for consensus DNA binding to p53 is relatively small, at approximately −0.5 kcal/mol·K, indicating no substantial conformational change upon DNA binding.

The contributions of enthalpy and entropy to the protein−DNA interaction can also be determined from the van't Hoff plot. The temperature at which $\Delta H = 0$, T_H, for p53−conDNA binding occurs at 15.2 °C, corresponding to the temperature at which the two species have the highest binding affinity over the range of temperatures studied (Figure 8). However, the temperature at which $\Delta S = 0$, T_S, is 40 °C, indicating that the most thermodynamically favorable temperature for complex formation (i.e., most negative ΔG) occurs near physiological temperature. Below T_H, the interaction is driven by entropy since the enthalpy term is positive in this region. Above T_S, 40 °C, the ΔS term becomes negative (and thus, $-T\Delta S$ becomes positive), and the interaction is driven by enthalpy (eq 6). At all temperatures between T_H and T_S, both enthalpic and entropic forces drive the p53−DNA interaction. Evident in Figure 8 is the absence of significant changes in the free energy of binding across the temperatures investigated, with a total differential of only ∼1.2 kcal/mol.

p53 Remains Tetrameric at 50 °C. Glutaraldehyde cross-linking experiments, previously reported to monitor p53 assembly state (*70*), were used to determine whether the 6-fold loss of DNA binding affinity from room temperature to 50 °C was related to the inability of the protein to form tetramers. Incubation of p53 with glutaraldehyde at either room temperature or 50 °C followed by SDS−PAGE resulted in a cross-linked protein band of ∼200 000 Da, an expected value for tetrameric p53 (Figure 9). These bands were reactive with the p53 monoclonal antibody Ab240. While glutaraldehyde cross-linking occurs on a faster time scale at 50 °C than at room temperature, the final amounts of tetrameric p53 observed are similar.

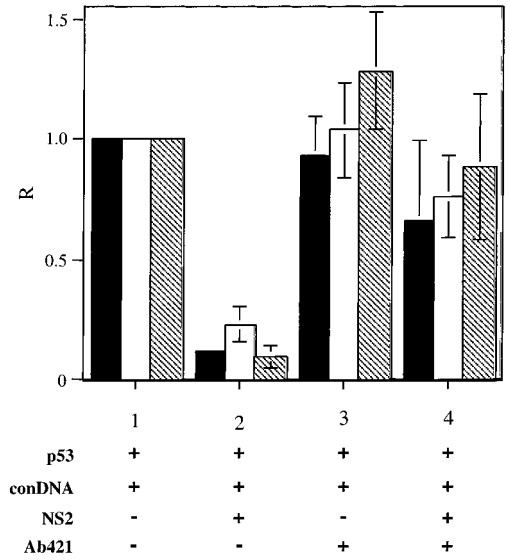

FIGURE 6: Effects of nonspecific DNA and Ab421 on binding to consensus DNA at 0, 22, and 50 °C. p53 at 1×10^{-8} M (tetramer) was mixed with radiolabeled consensus DNA at 2×10^{-11} M. Nonspecific DNA (unlabeled) was added to 2×10^{-6} M to determine its effect on p53−conDNA binding. Significant inhibition of binding is evident at all three temperatures assayed (condition 2). Addition of 2.4×10^{-8} M Ab421 antibody alone did not significantly alter the binding of purified full-length p53 to conDNA (condition 3). However, addition of Ab421 to the mixture of labeled conDNA and unlabeled nonspecific DNA restored conDNA binding to a significant degree (condition 4). By design, these experiments are very sensitive to small variations in reaction components; as a consequence, the error range is large, and no distinctions between 0 °C (solid bar), 22 °C (plain bar), and 50 °C (diagonally striped bar) were detectable. Data are reported as a fraction relative to conDNA binding to p53 alone at each temperature and errors bars indicate one standard deviation.

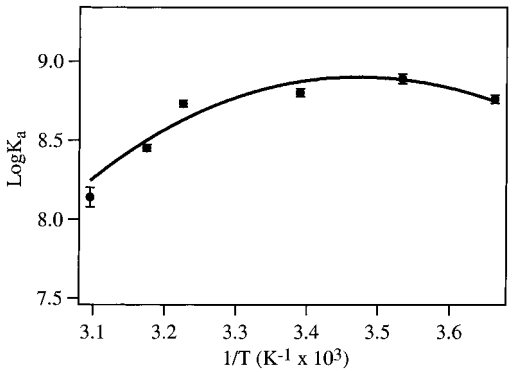

FIGURE 7: van't Hoff plot of DNA binding data. The fit (solid line) to the data points generated from binding isotherms yields the thermodynamic parameters, ΔC_p, T_H, T_S, of p53 binding to conDNA (see text). The slight curvature of the fit highlights the small change in binding affinity over the temperatures studied and corresponds to a ΔC_p of approximately −0.5 kcal/mol·K. Error bars indicate one standard deviation.

Antibody Reactivity Does Not Follow DNA Binding Activity at Elevated Temperatures. The accessibility of an epitope in the DNA binding domain of p53 was assayed at the temperatures at which significant DNA binding was demonstrated. Monoclonal antibody Ab1620 has been used previously to monitor a region in the core domain of p53 between residues 88 to 109 that is presumed to be exposed only in the wild-type conformation but is not available in mutant or unfolded p53 (*47*, *50*). The loss of the Ab1620 epitope at temperatures >37 °C in full-length p53 protein

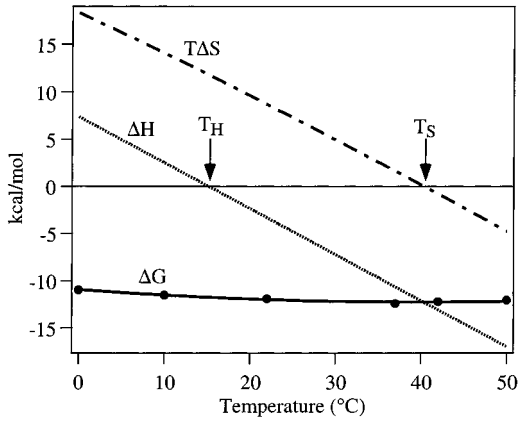

FIGURE 8: Determination of the contributions of ΔH and ΔS to the Gibbs free energy change for p53−dsDNA binding. Values of ΔC_p determined from the fit of the data presented in Figure 7 were used according to eqs 3−5 to determine the contributions of ΔH (dotted line) and $T\Delta S$ (dashed line) to ΔG. T_H (15 °C) and T_S (40 °C) are marked to illustrate the tightest binding and most favorable ΔG, respectively. The solid line corresponds to ΔG determined by $\Delta G = \Delta H - T\Delta S$, and the data points were determined by $\Delta G_{obs} = -RT\ln K_{obs}$. Note the small change (~1.2 kcal/mol) for ΔG_{obs} over these temperatures.

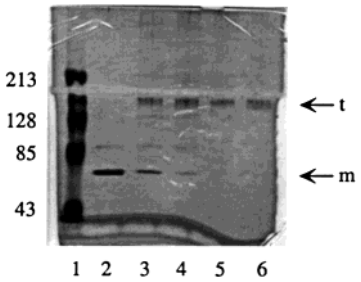

FIGURE 9: Glutaraldehyde cross-linking of p53 at room temperature and 50 °C. Purified p53 was incubated at either room temperature (lanes 3 and 5) or 50 °C (lanes 4 and 6) in the presence of 0.01% glutaraldehyde to verify the presence of tetrameric p53 in solution. At both temperatures, samples were allowed to incubate for 5 min (lanes 3 and 4) or 20 min (lanes 5 and 6) before being prepared for electrophoresis. Molecular weight markers in lane 1 are expressed in kDa, and lane 2 contains purified p53 in the absence of glutaraldehyde. Arrows mark monomeric (m), and tetrameric (t), forms of p53. Both species were reactive to p53 monoclonal antibody Ab240 (data not shown).

has been used to diagnose the presence of inactive protein, while positive reactivity has been used to indicate folded and active protein sample (*48*). In contrast, monoclonal antibody Ab421 is specific to an epitope in the C-terminus of p53 that is conformation-independent (*48*, *52*).

Ab1620 was able to recognize the purified protein after incubation at 0, 5, 16, 22, and 37 °C but not after incubation at 42, 50, or 65 °C (Figure 10). This result contrasts with the high affinity consensus dsDNA binding activity observed at both 42 and 50 °C (see Figure 5, panel A). Ab421 was positive for samples at all temperatures assayed. The antibody binding results are consistent with those reported previously (*48*), but the CD and DNA binding studies indicate that Ab1620 reaction does not correlate directly with the folding or activity of the full-length protein.

DISCUSSION

The critical response of p53 accumulation to the stimulus of DNA damage is generated by inhibiting Mdm2-mediated

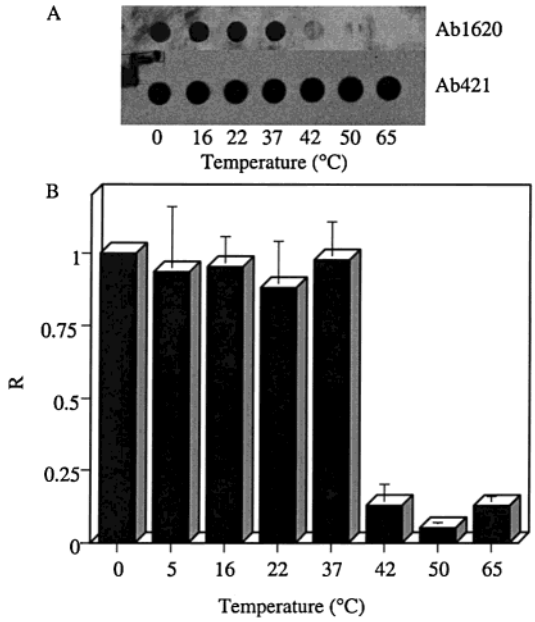

FIGURE 10: Conformational analysis via antibody reactivity as a function of temperature. (A) Protein was incubated at the indicated temperature for 30 min, filtered onto nitrocellulose, and exposed to either Ab1620 or Ab421 monoclonal p53 antibody. Radiography was used to detect antibody reactivity following ECL use (Amersham) to generate signal. (B) Densitometry was used to quantitate reactivity, and the results of at least three separate experiments at each temperature were averaged. Fractional reactivity (*R*) was determined at each temperature by comparison to reactivity at 0 °C. Error bars indicate one standard deviation.

degradation of p53 and/or stabilizing p53 structure (*28*, *35*−*39*). Modifications of the accumulated protein, including phosphorylation and acetylation, have appeared essential to "activate" high affinity DNA site recognition (*6*, *29*, *31*−*33*, *48*). However, studies on the full-length p53 protein without posttranslational modification have been incomplete. The ability of this unmodified protein to recognize the p53 dsDNA consensus sequence has not been assessed in the absence of nonspecific DNA competitors that have been shown to interfere with specific binding (*40*, *41*). We therefore sought to examine thermal stability and DNA binding capacity, both central to understanding structure and function of p53, using full-length protein produced in *Escherichia coli* and therefore lacking posttranslational modifications characteristic of eukaryotic organisms.

Previous studies have indicated that p53 is relatively unstable at physiological temperatures, suggesting that thermodynamic instability of the full-length protein may play a role in regulating p53 cellular response (*44*, *45*, *48*, *50*, *51*). Consistent with this view, thermodynamic comparison of DNA binding domain peptides derived from p53 mutants has indicated that protein conformation and stability are crucial to the function of this tumor suppressor protein (*49*, *71*, *72*). To address directly the question of thermodynamic stability of full-length p53 protein, we measured circular dichroism spectra as a function of temperature. The spectra were compared to results from predicted secondary structure algorithms and to solved structures of four p53 fragments. Using this approach, the vast majority of β-sheet structure in the full-length protein can be assigned to the DNA binding domain. This β-sheet CD signal corresponding to the DNA binding domain is remarkably stable to very high temperatures. The estimated midpoint of the irreversible unfolding for the full-length protein is 73 °C, significantly higher than that observed for the DNA binding domain as an isolated fragment (42 °C) (*49*).

This increased thermostability of the p53 DNA binding domain in the context of the full-length protein may result from a variety of factors, in particular oligomer formation. Previously published unfolding results investigating the stability of the tetramerization domain as a fragment determined a melting temperature of ~75−80 °C for this α-helical motif, suggesting that p53 may remain tetrameric up to this temperature (*73*, *74*). Because the β-sheet structure signal of the much larger DNA binding domain overwhelms the expected CD signal for the small α-helical tetramerization domain, we are unable to confirm the presence of this α-helical region at elevated temperatures. However, glutaraldehyde cross-linking results indicate that the protein remains tetrameric to 50 °C. The persistence of tetramer and the high T_m of the tetramerization domain lead us to propose that the observed loss of α-helical CD signal at elevated temperatures represents unfolding of the p53 N-terminus and the unstable C-terminal α-helix that binds S100B (*62*) rather than the tetramerization domain. The N-terminal region is predicted to have both α-helical and large random coil regions (see Figure 2), and biochemical experiments suggest that this region is not highly structured (*75*).

The fold of the p53 β-sheet DNA binding domain is not common among DNA binding proteins and may provide potential for interactions that increase stability of the full-length protein relative to the isolated DNA binding domain. The β-sheet structure within the monomer may be extended to form additional inter-monomeric β-sheet associations that stabilize the tetramer. Indeed, DNA bending that enhances p53 affinity for its DNA target site (*76*−*78*) may also increase monomer−monomer interactions. Interactions between various domains of p53 may also contribute to the enhanced stability of the core DNA binding domain in the full-length protein. Although widely separated in the primary sequence, thermal studies of deletion mutants indicate that the N- and C-terminal domains influence activity of the folded protein (*79*). Additionally, alterations in the N-terminal domain can influence the properties of the DNA binding domain, further illustrating that a variety of interactions may contribute to the increased stability of the full-length protein (*8*).

The ability of the DNA binding domain to recognize specific sites on dsDNA is a critical property for p53 function as a regulator of transcription. The apparent p53 requirement for "activation" of high affinity DNA binding by a variety of agents gave rise to the "latent-activated" conformational hypothesis for p53 function (*31*−*33*). However, more recent experiments demonstrate that the observed increase in p53 binding to consensus dsDNA sequences in response to activating agents derives, at least in part, from releasing the inhibitory effect of nonspecific DNA in the assay mixtures employed (*40*, *41*). To explore the inherent ability of p53 without "activation" to recognize its consensus dsDNA target, we have examined the DNA binding properties of full-length p53 isolated from *Escherichia coli*. High affinity binding (K_d ~ 1.6×10^{-9} M_{tet}) of the bacterially grown, "latent" form of the protein to a 20 bp dsDNA consensus sequence for p53 dispels the view that this protein requires activation for

effective DNA binding. The binding affinity for consensus DNA determined in this work is comparable to the highest affinities reported previously for an "activated" form of the protein that was generated by C-terminal truncation (*80*). Thus, the requirement for "activation" does not derive from compensation for an inherent deficit in the DNA binding capacity of the unmodified protein, but rather from inhibition by competing nonspecific dsDNA. This competition was clearly demonstrated upon addition of nonspecific DNA (NS2) to p53-conDNA. Further, the addition of the "activator" Ab421 had no significant effect on specific DNA binding in the absence of nonspecific DNA but restored p53-conDNA binding in the presence of NS2. These studies confirm that the activation requirement for "latent" p53 to bind specific dsDNA is dependent on the presence of competing nonspecific DNA and does not reflect a deficit in the ability of purified unmodified protein to bind conDNA (*40*, *41*).

The demonstrated thermal stability of secondary structure corresponding to the DNA binding domain suggested the possibility that DNA binding might also persist to high temperature in the full-length protein. In the absence of nonspecific competitor DNA, "latent" p53 is not only active at physiological temperature but retains high affinity binding to temperatures as high as 50 °C with only a 5−6-fold decrease in affinity for conDNA. This loss in affinity does not derive from a decrease in the fraction of active protein, as stoichiometric assays at room temperature and 50 °C yield similar levels of active protein. The decrease in affinity at 50 °C is also not due to a switch to nonspecific binding, since p53 binding to a nonspecific sequence (NS2) results in an apparent affinity substantially less that of conDNA at 50 °C. Further, the diminished activity at elevated temperature cannot be ascribed to alteration in oligomeric structure, as glutaraldehyde cross-linking assays demonstrate similar levels of tetrameric p53. The persistence of high affinity DNA binding in the full-length protein to at least 50 °C provides functional evidence that confirms the structural integrity of the β-sheet structure corresponding to the DNA binding domain.

A monoclonal antibody (Ab1620) has been deduced to react with only the "active" form of p53 and has been applied in numerous studies to assess thermal stability and predict the ability of p53 proteins to bind DNA with specificity (*32*, *45*, *46*, *48*, *50*). In our hands, reactivity with Ab1620 at elevated temperatures is similar to previously reported results (*48*): the epitope for this antibody is reactive at temperatures up to 37 °C, but no reactivity is observed above this temperature. However, this pattern does not track with direct measurements of DNA binding. One possibility is that Ab1620 detects a small conformational change that correlates with the 6-fold decrease in DNA binding observed over the temperature range examined; however, this alteration that abolishes the Ab1620 epitope does not completely abrogate DNA binding activity. Of importance for future studies is that reactivity with Ab1640 alone cannot be utilized to determine DNA binding capacity or the folded state of p53 with confidence.

Temperature dependence of protein−DNA binding has been used to assess the apolar surface area buried on formation of the complex (*56*, *81*). For DNA binding reactions in which protein folding is linked with complex formation, large negative changes in heat capacity of the reaction have been observed and attributed to a combination of both hydrophobic and hydrogen bonding forces (*56*, *81*, *82*). Interestingly, the temperature dependence of p53−conDNA binding suggests a relatively small change in the exposed apolar surface area upon complex formation (*56*, *81*). The ΔC_p for p53−conDNA interaction was determined to be approximately −0.5 kcal/mol·K. For comparison, *lac* repressor, another tetrameric DNA binding protein, exhibits a ΔC_p of −1.2 kcal/mol·K. This large ΔC_p for *lac* repressor is ascribed to the folding of the hinge domains of the protein concomitant with operator DNA binding (*81*). The relatively low value for p53−conDNA suggests that large alterations in protein fold or extensive changes in exposure of apolar residues to solvent are not associated with this binding interaction. A rough estimate of the number of amino acid side chains buried in this interaction, calculated from equations in ref *81* is ∼4 per monomer, a value that suggests minimal folding/rearrangement occurs in complex formation. The low ΔC_p value combined with the observed thermostability of the DNA binding domain in the intact protein suggests a relatively rigid fold for this domain that is able to "fit" the DNA binding surface without significant conformational alteration.

Motivation for this study was derived from the central importance of this tumor suppressor protein in vertebrate systems and the potential to employ p53 in cancer therapies based on structural and functional information. The results presented demonstrate unanticipated structural and functional stability for the DNA binding domain within the full-length unmodified p53 protein. These results contrast with earlier work that deduced lower stability and the requirement for activation of the protein for effective binding to its target DNA sites (*32*, *33*, *44*, *45*, *48*, *50*, *51*). The stability and function of p53 are influenced by interactions with multiple ligands—damaged DNA, dsDNA, ssDNA, and a multitude of other proteins—and modifications that include phosphorylation, acetylation, and alternative splicing (*6*, *7*). Demonstration that the sequence scaffold for p53 assumes a stable and highly functional structure in the absence of other modifications provides a baseline against which other studies can be compared. Of particular interest for the future will be assessment of the effects of modifications that have been deduced to affect p53 function in vivo (e.g., phosphorylation, acetylation, and amino acid substitutions) on the stability and inherent DNA binding capacity of this key regulatory protein.

ACKNOWLEDGMENT

The authors thank Dr. G. Lozano for the generous donation of p53 plasmids and hybridomas, Dr. S. Edmondson for critical discussion of CD results, E. Mrowczynski for work on p53 purification, and Dr. J. Nichols for assistance with structure visualization programs. We also thank M. Moraitis for assistance with data analysis and the Matthews laboratory for their comments and suggestions during the preparation of this manuscript.

REFERENCES

1. DeLeo, A. B., Jay, G., Appella, E., Dubois, G. C., Law, L. W., and Old, L. J. (1979) *Proc. Natl. Acad. Sci. U.S.A. 76*, 2420−2424.
2. Lane, D. P., and Crawford, L. V. (1979) *Nature 278*, 261−263.

3. Linzer, D. I. H., and Levine, A. J. (1979) *Cell 17*, 43−52.
4. Chang, C., Simmons, D. T., Martin, M. A., and Mora, P. T. (1979) *J. Virol. 31*, 463−471.
5. Kress, M., May, E., Cassingena, R., and May, P. (1979) *J. Virol. 31*, 472−483.
6. Levine, A. J. (1997) *Cell 88*, 323−331.
7. Albrechtsen, N., Dornreiter, I., Grosse, F., Kim, E., Wiesmüller, L., and Deppert, W. (1999) *Oncogene 18*, 7706−7717.
8. Prives, C., and Hall, P. A. (1999) *J. Pathol. 187*, 112−126.
9. Appella, E., and Anderson, C. W. (2000) *Pathol. Biol. 48*, 227−245.
10. Raycroft, L., Wu, H., and Lozano, G. (1990) *Science 249*, 1049−1051.
11. El-Deiry, W. S., Kern, S. E., Pietenpol, J. A., Kinzler, K. W., and Vogelstein, B. (1992) *Nat. Genet. 1*, 45−49.
12. Funk, W. D., Pak, D. T., Karas, R. H., Wright, W. E., and Shay, J. W. (1992) *Mol. Cell. Biol. 12*, 2866−2871.
13. Kastan, M. B., Zhan, Q., El-Deiry, W. S., Carrier, F., Jacks, T., Walsh, W. V., Plunkett, B. S., Vogelstein, B., and Fornace, A. J., Jr. (1992) *Cell 71*, 587−597.
14. Momand, J., Zambetti, G. P., Olson, D. C., George, D., and Levine, A. J. (1992) *Cell 69*, 1237−1245.
15. Foord, O., Navot, N., and Rotter, V. (1993) *Mol. Cell. Biol. 13*, 1378−1384.
16. El-Deiry, W. S. (1998) *Sem. Cancer Biol. 8*, 345−357.
17. Kern, S. E., Kinzler, K. W., Bruskin, A., Jarosz, D., Friedman, P., Prives, C., and Vogelstein, B. (1991) *Science 252*, 1708−1711.
18. Bargonetti, J., Friedman, P. N., Kern, S. E., Vogelstein, B., and Prives, C. (1991) *Cell 65*, 1083−1091.
19. Foord, O. S., Bhattacharya, P., Reich, Z., and Rotter, V. (1991) *Nucl. Acids Res. 19*, 5191−5198.
20. Bargonetti, J., Manfredi, J. J., Chen, X., Marshak, D. R., and Prives, C. (1993) *Genes Devel. 7*, 2565−2574.
21. Hernandez-Boussard, T., Rodriguez-Tome, P., Montesano, R., and Hainaut, P. (1999) *Hum. Mutat. 14*, 1−8.
22. Soussi, T., Dehouche, K., and Béroud, C. (2000) *Hum. Mutat. 15*, 105−113.
23. Scheffner, M., Nuber, U., and Huibregtse, J. M. (1995) *Nature 373*, 81−83.
24. Maki, C. G., Huibregtse, J. M., and Howley, P. M. (1996) *Cancer Res. 56*, 2649−2654.
25. Haupt, Y., Maya, R., Kazaz, A., and Oren, M. (1997) *Nature 387*, 296−299.
26. Honda, R., Tanaka, H., and Yasuda, H. (1997) *FEBS Lett. 420*, 25−27.
27. Kubbutat, M. H. G., Jones, S. N., and Vousden, K. H. (1997) *Nature 387*, 299−303.
28. Momand, J., Wu, H.-H., and Dasgupta, G. (2000) *Gene 242*, 15−29.
29. Maltzman, W., and Czyzyk, L. (1984) *Mol. Cell. Biol. 4*, 1689−1694.
30. Lu, X., and Lane, D. P. (1993) *Cell 75*, 765−778.
31. Milner, J. (1991) *Proc. Royal Soc. London B Biol. Sci. 245*, 139−145.
32. Halazonetis, T. D., Davis, L. J., and Kandil, A. N. (1993) *EMBO J. 12*, 1021−1028.
33. Hupp, T. R., and Lane, D. P. (1994) *Cur. Biol. 4*, 865−875.
34. Jayaraman, L., and Prives, C. (1995) *Cell 81*, 1021−1029.
35. Blaydes, J. P., Gire, V., Rowson, J. M., and Wynford-Thomas, D. (1997) *Oncogene 14*, 1859−1868.
36. Midgley, C. A., and Lane, D. P. (1997) *Oncogene 15*, 1179−1189.
37. Blaydes, J. P., and Wynford-Thomas, D. (1998) *Oncogene 16*, 3317−3322.
38. Chen, L., Agrawal, S., Zhou, W., Zhang, R., and Chen, J. (1998) *Proc. Natl. Acad. Sci. U.S.A. 95*, 195−200.
39. de Rozieres, S., Maya, R., Oren, M., and Lozano, G. (2000) *Oncogene 19*, 1691−1697.
40. Bayle, J. H., Elenbaas, B., and Levine, A. J. (1995) *Proc. Natl. Acad. Sci. U.S.A. 92*, 5729−5733.
41. Anderson, M. E., Woelker, B., Reed, M., Wang, P., and Tegtmeyer, P. (1997) *Mol. Cell. Biol. 17*, 6255−6264.
42. Oren, M., Maltzman, W., and Levine, A. J. (1981) *Mol. Cell. Biol. 1*, 101−110.
43. Hall, A. R., and Milner, J. (1997) *Oncogene 14*, 1371−1376.
44. Friedlander, P., Legros, Y., Soussi, T., and Prives, C. (1996) *J. Biol. Chem. 271*, 25468−25478.
45. Hainaut, P., Butcher, S., and Milner, J. (1995) *Br. J. Cancer 71*, 227−231.
46. Milner, J., Cook, A., and Sheldon, M. (1987) *Oncogene 1*, 453−455.
47. Cook, A., and Milner, J. (1990) *Br. J. Cancer 61*, 548−552.
48. Hansen, S., Hupp, T. R., and Lane, D. P. (1996) *J. Biol. Chem. 271*, 3917−3924.
49. Bullock, A. N., Henckel, J., DeDecker, B. S., Johnson, C. M., Nikolova, P. V., Proctor, M. R., Lane, D. P., and Fersht, A. R. (1997) *Proc. Natl. Acad. Sci. U.S.A. 94*, 14338−14342.
50. Milner, J., and Medcalf, E. A. (1990) *J. Mol. Biol. 216*, 481−484.
51. Ponchel, F., and Milner, J. (1998) *Br. J. Cancer 77*, 1555−1561.
52. Harlow, E., Crawford, L. V., Pim, D. C., and Williamson, N. M. (1981) *J. Virol. 39*, *861*−*869*.
53. Gannon, J. V., Greaves, R., Iggo, R., and Lane, D. P. (1990) *EMBO J. 9*, 1595−1602.
54. Bradford, M. M. (1976) *Anal. Biochem. 72*, 248−254.
55. Wong, I., and Lohman, T. M. (1993) *Proc. Natl. Acad. Sci. U.S.A. 90*, 5428−5432.
56. Ha, J.-H., Spolar, R. S., and Record, M. T., Jr. (1989) *J. Mol. Biol. 209*, 801−816.
57. Kussie, P. H., Gorina, S., Marechal, V., Elenbaas, B., Moreau, J., Levine, A. J., and Pavletich, N. P. (1996) *Science 274*, 948−953.
58. Cho, Y., Gorina, S., Jeffrey, P. D., and Pavletich, N. P. (1994) *Science 265*, 346−355.
59. Lee, W. T., Harvey, T. S., Yin, Y., Yau, P., Litchfield, D., and Arrowsmith, C. H. (1994) *Nat. Struct. Biol. 1*, 877−890.
60. Clore, G. M., Ernst, J., Clubb, R., Omichinski, J. G., Kennedy, W. M. P., Sakaguchi, K., Appella, E., and Gronenborn, A. M. (1995) *Nat. Struct. Biol. 2*, 321−333.
61. Jeffrey, P. D., Gorina, S., and Pavletich, N. P. (1995) *Science 267*, 1498−1502.
62. Rustandi, R. R., Baldisseri, D. M., and Weber, D. J. (2000) *Nat. Struct. Biol. 7*, 570−574.
63. Chou, P. Y., and Fasman, G. D. (1978) *Adv. Enzymol. 47*, 45−148.
64. Garnier, J., Osguthorpe, D. J., and Robson, B. (1978) *J. Mol. Biol. 120*, 97−120.
65. Burgess, A. W., Ponnuswany, P. K., and Sheraga, H. A. (1974) *Isr. J. Chem. 12*, 239−286.
66. Deléage, G., and Roux, B. (1987) *Protein Eng. 1*, 289−294.
67. Holley, L. H., and Karplus, M. (1989) *Proc. Natl. Acad. Sci. U.S.A. 86*, 152−156.
68. Garnier, J., Gilbrat, J.-F., and Robson, B. (1996) *Methods Enzymol. 266*, 540−553.
69. King, R. D., and Sternberg, M. J. E. (1996) *Protein Sci. 5*, 2298−2310.
70. Friedman, P. N., Chen, X., Bargonetti, J., and Prives, C. (1993) *Proc. Natl. Acad. Sci. U.S.A. 90*, 3319−3323.
71. Wong, K.-B., DeDecker, B. S., Freund, S. M. V., Proctor, M. R., Bycroft, M., and Fersht, A. R. (1999) *Proc. Natl. Acad. Sci. U.S.A. 96*, 8438−8442.
72. Bullock, A. N., Henckel, J., and Fersht, A. R. (2000) *Oncogene 19*, 1245−1256.
73. Johnson, C. R., Morin, P. E., Arrowsmith, C. H., and Freire, E. (1995) *Biochemistry 34*, 5309−5316.
74. Mateu, M. G., and Fersht, A. R. (1998) *EMBO J. 17*, 2748−2758.
75. Pavletich, N. P., Chambers, K. A., and Pabo, C. O. (1993) *Genes Dev. 7*, 2556−2564.
76. Nagaich, A. K., Appella, E., and Harrington, R. E. (1997) *J. Biol. Chem. 272*, 14842−14849.
77. Balagurumoorthy, P., Sakamoto, H., Lewis, M. S., Zambrano, N., Clore, G. M., Gronenborn, A. M., Appella, E., and Harrington, R. E. (1995) *Proc. Natl. Acad. Sci. U.S.A. 92*, 8591−8595.

78. Cherny, D. I., Striker, G., Subramaniam, V., Jett, S. D., Palecek, E., and Jovin, T. M. (1999) *J. Mol. Biol. 294*, 1015−1026.
79. Hansen, S., Lane, D. P., and Midgley, C. A. (1998) *J. Mol. Biol. 275*, 575−588.
80. Wang, Y., Schwedes, J. F., Parks, D., Mann, K., and Tegtmeyer, P. (1995) *Mol. Cell. Biol. 15*, 2157−2165.
81. Spolar, R. S., and Record, M. T., Jr. (1994) *Science 263*, 777−784.
82. Cooper, A. (2000) *Biophys. Chem. 85*, 25−39.
83. Carson, M. (1997) *Methods Enzymol. 277*, 493−505.

BI002088Z